Optical remote sensing of sound in the ocean

James H. Churnside
Konstantin Naugolnykh
Richard D. Marchbanks

Optical remote sensing of sound in the ocean

James H. Churnside,[a,*] Konstantin Naugolnykh,[b] and Richard D. Marchbanks[c]

[a]NOAA Earth System Research Laboratory, 325 Broadway, Boulder, Colorado 80305-3337, United States
[b]Zel Technologies, 325 Broadway, Boulder, Colorado 80305-3337, United States
[c]NOAA and University of Colorado, Cooperative Institute for Research in the Environmental Sciences, 325 Broadway, Boulder, Colorado 80305-3337, United States

Abstract. We propose a remote sensing technique to measure sound in the upper ocean. The objective is a system that can be flown on an aircraft. Conventional acoustic sensors are ineffective in this application, because almost none (∼0.1%) of the sound in the ocean is transmitted through the water/air interface. The technique is based on the acoustic modulation of naturally occurring bubbles near the sea surface. It is clear from the ideal gas law that the volume of a bubble will decrease if the pressure is increased, as long as the number of gas molecules and temperature remain constant. The pressure variations associated with the acoustic field will therefore induce proportional volume fluctuations of the insonified bubbles. The lidar return from a collection of bubbles is proportional to the total void fraction, independent of the bubble size distribution. This implies that the lidar return from a collection of insonified bubbles will be modulated at the acoustic frequencies, independent of the bubble size distribution. Moreover, that modulation is linearly related to the sound pressure. A laboratory experiment confirmed the basic principles, and estimates of signal-to-noise ratio suggest that the technique will work in the open ocean. © *The Authors. Published by SPIE under a Creative Commons Attribution 3.0 Unported License. Distribution or reproduction of this work in whole or in part requires full attribution of the original publication, including its DOI.* [DOI: 10.1117/1.JRS.9.096038]

1 Introduction

There are a number of reasons one might want to fly over the ocean and listen to the sound below the surface. Examples include measurement of shipping noise, tracking of marine mammals, and searching for the flight data recorder of a lost aircraft, like Malaysian Airlines flight MH370. Unfortunately, direct detection of sound from above is difficult because the transmission loss at the surface is 65 dB. The transmission loss at the surface for visible light is only ∼0.1 dB, so a technique that uses visible light to interrogate the acoustic field just below the surface would be desirable.

Fabrikant suggested modulating a laser such that the wavelength of the modulation was Bragg-matched to the acoustic wavelength in water.[1] Small variations in the optical scattering induced by the acoustic wave would cause amplitude modulation of the scattered light. He showed how an acoustic wave moving toward the surface would produce a signal at the modulation frequency with a Doppler shift determined by the speed of sound.

Others have suggested using coherent optical detection of the light reflected from the sea surface to directly measure the motion of the surface induced by the acoustic pressure, and this technique has been demonstrated in laboratory tests.[2–4] The motion of the surface induced by the acoustic signal can be much smaller than the motion induced by surface winds, and separating the two effects using this technique can be difficult. One technique to accomplish this is to

---

measure the statistical properties of the scattered laser light, which are affected by the acoustic signal.[5,6] This technique has also been demonstrated in a laboratory setting, but the application of this technique in the open ocean would be difficult.

This paper suggests another approach. Light scattered from bubbles that are always present near the ocean surface will be modulated at acoustic frequencies when the size of those bubbles is modulated by the pressure associated with the acoustic field. Airborne lidar can penetrate the air/sea interface into the near-surface layer of the ocean. This near-surface layer is where the bubble concentration is greatest.[7,8] Sound can propagate up from great depths to near the surface, so this technique has the potential to detect sound sources that are well below the penetration depth of an airborne lidar.

2 Theoretical Background

If the frequency of sound is much less than the resonant frequency of a bubble, its relative volume will change adiabatically with a small change in pressure as

$$\frac{\Delta V}{V} = -\frac{1}{\gamma}\frac{\Delta P}{P},\tag{1}$$

where γ, the ratio of specific heat at constant pressure to that at constant volume, is 1.4 for air.

The resonance frequency is given by[9]

$$f_0 = \frac{1}{2\pi a}\left(\frac{3\gamma P}{\rho}\right)^{\frac{1}{2}} = \frac{3.2\text{ m s}^{-1}}{a},\tag{2}$$

where a is the bubble radius and ρ is the density of seawater. The numerical value uses the pressure near the surface ($P = 10^5$ Pa) and density $\rho = 1029$ kg m^{-3}. At the resonance frequency, the relative volume change is enhanced by a factor that is equal to the bubble quality factor Q, where

$$Q \cong \frac{75}{1 + 0.033 f_0^{0.5}}\tag{3}$$

for bubble radii between $\sim$30 μm and 3 mm.[9]

For a fixed frequency and a distribution of bubble sizes, bubbles that are at resonance and those not at resonance must be treated separately and the results added. Since Q is the ratio of f_0 to the width of the resonance, a bubble will be in resonance for frequencies in the range

$$f = f_0\left(1 \pm \frac{1}{2Q}\right).\tag{4}$$

This implies that, for a frequency f, bubbles within the size range of

$$a = \frac{1}{2\pi f\left(1 \pm \frac{1}{2Q}\right)}\left(\frac{3\gamma P}{\rho}\right)^{\frac{1}{2}} = \frac{3.2\text{ m s}^{-1}}{f\left(1 \pm \frac{1}{2Q}\right)}\tag{5}$$

should be treated as resonant and those outside this range as nonresonant.

The lidar signal S is proportional to the volume scattering function β at the lidar scattering angle of π radians. Using geometric optics, it is straightforward to show that the latter quantity is proportional to the void fraction F_v of the bubbles within the lidar resolution element independent of the bubble size distribution.[10] Neglecting possible resonance effects, the modulation depth of the lidar signal can be expressed as

$$M = \frac{\Delta S}{S} = \frac{1}{\gamma}\frac{\Delta P}{P}\tag{6}$$

as long as the acoustic pressure is constant within the illuminated volume. If some fraction, η, of the bubbles are within the resonance range, this should be increased so

$$M = \frac{1}{\gamma} \frac{\Delta P}{P} (1 - \eta + \eta\,Q). \tag{7}$$

Because the sound wave is almost totally reflected from the surface with a phase reversal, a standing wave is produced. The resulting acoustic pressure $\Delta P(z)$ from an incident acoustic wave with wavenumber k_a and amplitude P_a is

$$\Delta P(z) = 2P_a \, \sin(k_a z). \tag{8}$$

The factor of two comes from the superposition of the incident and reflected acoustic wave. This has a maximum at a depth of $0.25\lambda_a$, where λ_a is the acoustic wavelength. For a plane wave and flat surface, this same maximum value also occurs at $0.75\lambda_a$, $1.25\lambda_a$, and so on. However, this complete interference is not always observed in practice because of surface roughness, bubbles, and bottom reflections.[11,12]

To be detectable, the modulation depth has to be greater than the relative fluctuations caused by noise processes. For a shot-noise-limited system, this implies that the minimum detectable sound pressure level is given by

$$\Delta P > \gamma P \left(\frac{2eB}{S} \right)^{\frac{1}{2}}, \tag{9}$$

where e is the electronic charge, B is the receiver noise bandwidth (spectral resolution), and the signal S is the average photocathode current. Near the sea surface, we can write this requirement in terms of the acoustic sound pressure and signal-to-noise ratio (SNR) in dB as

$$\Delta P(\text{dB re 1 } \mu\text{Pa}) > 223 \text{ dB} - \text{SNR(dB)}. \tag{10}$$

3 Experiment Description

These concepts were tested in a laboratory tank (Fig. 1) with a bubbler and speaker on the bottom and a laser source and optical receiver at the side of the clear glass tank. The tank itself is 60 cm wide by 180 cm long and was filled with water to a depth of 70 cm. The measurement volume was located 24 cm below the surface at a distance of 25 cm from one side of the tank.

A plume of bubbles was produced by running compressed air through a ceramic filter (Sweetwater air diffuser model ALR150, 152 by 38 by 38 mm) with void fraction controlled by controlling the flow of air to the filter. This was oriented with the long axis vertical to produce a bubble plume that was nearly circular at the measurement volume with a diameter of 50 mm. This technique was chosen to get a relatively narrow bubble size distribution.[13] For low void fraction, the actual size distribution and void fraction were measured using photographs of the
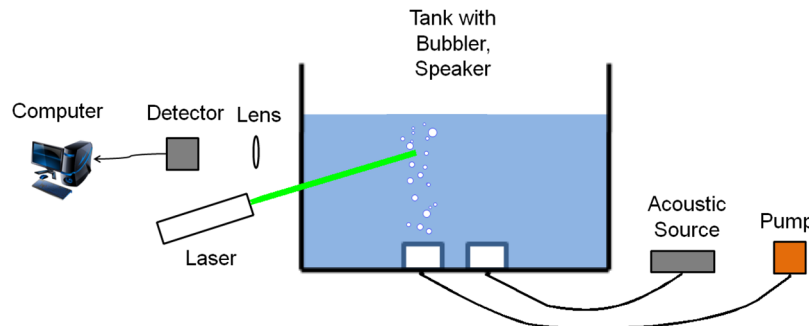

Fig. 1 Schematic diagram of the tank experiment. A bubbler on the bottom is supplied with compressed air from a pump. A speaker is driven with a 5 kHz acoustic source. The laser beam illuminates the bubble plume from outside the tank, and a lens collects a portion of the scattered light onto a photodetector.
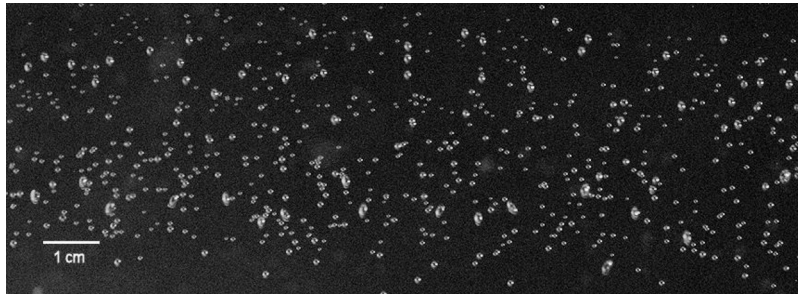
Fig. 2 Example of contrast-enhanced bubble photograph used to measure void fraction and size distribution.

bubble plume (Fig. 2). For each photograph, the contrast was enhanced, and then the area of each bubble was measured and converted to radius and volume.

The average of the distributions from seven photographs (Fig. 3) shows a peak in the bin where 0.45 mm $< a <$ 0.5 mm. The average radius was 0.61 mm and the rms width of the distribution was 0.20 mm. The void fraction was measured from those same images using the thickness of the plume, with a result of $(1.17 \pm 0.12) \times 10^{-3}$.

At higher void fractions, the bubbles in the photographs could not be resolved, so another technique was used to estimate void fraction. The average bubble rise velocity was estimated from the smearing in a long-exposure photograph (20 ms), and the void fraction estimated from the bubble plume diameter, average bubble rise velocity, and the measured flow rate of air to the diffuser. Using this technique, the flow rate was adjusted to obtain a void fraction of 0.01.

A 5 kHz acoustic signal was generated digitally with 100 samples per cycle and an amplitude resolution of 16 bits. This was converted to an analog voltage, amplified, and sent to an underwater speaker suspended just above the bottom of the tank. The sound pressure was measured at the measurement volume with a hydrophone. Any effects of interference between the direct and reflected acoustic pressures are taken into account in this measurement.

The sound pressure levels were measured with an Aquarian Audio Products H1A hydrophone, which has a typical response of -200 dB re 1 V μPa^{-1} at 5 kHz. At low void fraction, the measured sound pressure level at the measurement position was linearly proportional to the drive voltage with a response of 1423 Pa V^{-1}. At higher void fraction, the sound pressure levels are reduced by attenuation by the bubble plume and are difficult to measure directly. To first order, this reduction should be proportional to the ratio of the void fractions for the two cases (a factor of 8.55), so the sound pressure at high void fraction was taken to be proportional to the drive voltage with a response of 166 Pa V^{-1}.
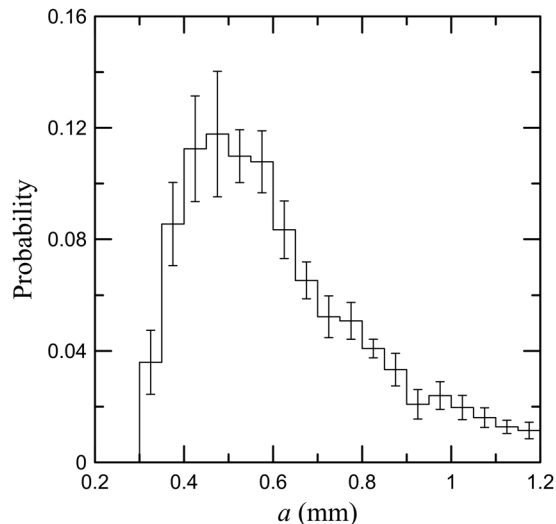

Fig. 3 Histogram of bubble radius, a. Error bars represent the standard deviation of values from the seven photographs.

The optical source was a 40 mW stabilized laser operating at a wavelength of 532 nm. The beam was expanded to a diameter of 30 mm at the measurement volume with a diverging lens. The receiver used a lens to collect the scattered light onto a photodiode. The field of view of the receiver at the measurement volume was 31 mm. To reduce the amount of scattering from the tank, the receiver was offset at an angle of 16 deg from the transmitted beam.

The photodiode output was converted to a voltage with a transimpedance amplifier. The resulting voltage was sampled at 41 kHz by the 24-bit computer sound card to obtain the acoustic modulation. For each sound pressure, the power spectral density was calculated for 100 consecutive data segments that were each 1 s long (1 Hz spectral resolution). The same voltage was also sampled at 100 Hz by a dc coupled digitizer to obtain the average return. The modulation depth was calculated as

$$M = \frac{[\overline{\text{PSD}}(5 \text{ kHz}) - \overline{\text{PSD}}(4.5 \text{ kHz})]^{1/2}}{S_0}, \quad (11)$$

where the overbar denotes the average of the 100 spectra, and S_0 is the average dc signal at zero sound pressure level. Errors were estimated for an averaging time of 10 s using the variance of the 100 spectra at 4.5 and 5 kHz.

4 Laboratory Results

A typical power spectral density of the optical signal (Fig. 4) shows a very narrow spectral peak at 5 kHz. Q is 22.5 at this frequency. The sound pressure level, estimated using the manufacturer's response, was 1700 Pa. SNR inferred from the plot is 57 dB.

For low void fraction, the measured modulation depth (Fig. 5) shows a clear increase in modulation depth with increasing sound pressure. The response is very nearly linear, except at the very lowest sound levels, where detector noise is an issue. One interesting feature of the three lowest points is the relatively small error bars; the variability of the detector noise on time scales of several seconds is much less than the variability in the bubble plume. From a linear regression, the slope of the response is $(1.08 \pm 0.04) \times 10^{-5}$ Pa^{-1}. The theoretical response in the figure, from Eq. (6), has a slope of 7.14×10^{-6} Pa^{-1}. This difference is not within the statistical uncertainty of the regression, but is within the uncertainty in the hydrophone calibration (± 4 dB).
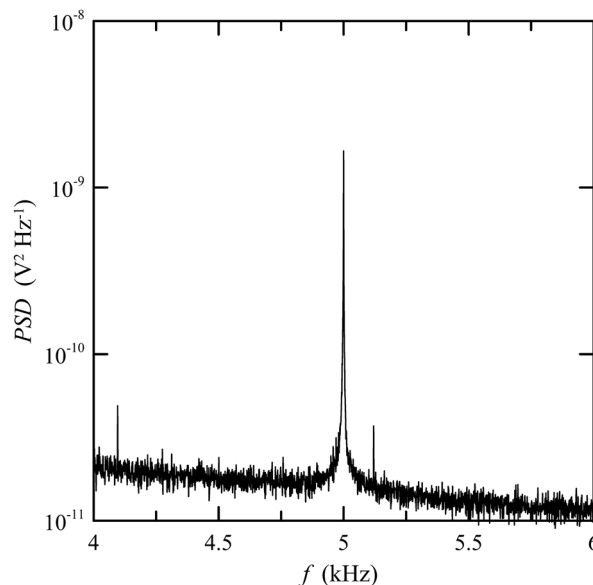

Fig. 4 Example of the power spectral density function of the optical detector output as a function of frequency, f, for the low-void-fraction case.
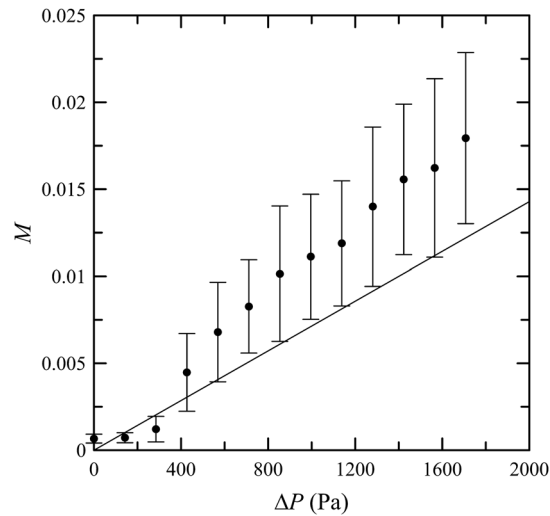
Fig. 5 Modulation depth, M, as a function of sound pressure amplitude, ΔP, for low-void fraction. Circles are averages of ten 1-s measurements, error bars represent the standard deviation of those measurements, and the solid line is the theoretical prediction.

Fig. 6 Modulation depth, M, as a function of sound pressure amplitude, ΔP, for high-void fraction. Circles are averages of ten 1-s measurements, error bars represent the standard deviation of those measurements, and the solid line is the theoretical prediction.
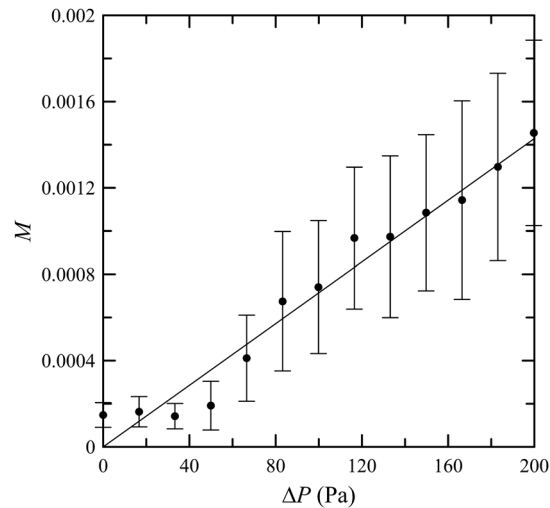
For the higher void fraction, the measured modulation depth (Fig. 6) looks very similar, except that both sound pressure levels and modulation depths are roughly an order of magnitude lower as a result of the greater attenuation by the bubble plume. Here, the slope of the regression is $(7.14 \pm 0.41) \times 10^{-6}$ Pa^{-1}, and the close agreement with the theoretical value is largely coincidental. At this void fraction, more light is scattered by the bubble plume, so the signal to noise is greater and the modulation is visible above the noise at a lower sound pressure. The ratio of minimum detectable signals for the two cases is 6.4, or ~75% of the expected value based on the ratio of void fractions.

5 System Considerations

The lidar system needed to measure sound in the open ocean is different from existing systems, where the objective is to measure the vertical distribution of scattering particles like fish[14,15] and plankton[16] in the water or to use the distribution of plankton to infer dynamical processes like

internal waves.[17–19] Such systems require a high instantaneous dynamic range and often use polarization to enhance the return.[20,21] An acoustic detection lidar, on the other hand, does not benefit from the use of polarization, since the return from bubbles preserves polarization.[10] A high dynamic range is not required, since the system only requires a single sample of the return from each transmitted pulse, at a constant depth, and this can be made near the surface. What is required is (1) a relatively high pulse-repetition rate in order to sample the return at acoustic frequencies and (2) a high SNR to measure the small modulation depths expected.

The SNR will generally be limited by shot noise in the photocurrent, which depends on the near-surface bubble void fraction.[10] In bubble clouds associated with breaking waves, values between 10^{-4} and 0.01 have been observed.[22–24] The background void fraction is much lower. Thorpe et al.[25] reported values between 10^{-8} and 10^{-7} at depths of 2 to 4 m and winds near 10 m s^{-1}. Vagle et al.[26] present a probability distribution of measured values that shows most of the values between 10^{-8} and 10^{-6}, with the most likely value just larger than 10^{-7}. Gemmrich[27] measured void fraction at depths of 2.6 and 0.85 m between and within the convergence zone of Langmuir circulation. At the deeper location, the background void fraction was $<10^{-7}$, increasing to $>10^{-6}$ in the convergence. At the shallower location, the background was $\approx 5 \times 10^{-6}$, increasing to just under 10^{-4} in the convergence.

There are always some bubbles present, but most are produced by wind–wave interactions. An empirical model[28] predicts void fraction of

$$F_V = 4.65 \times 10^{-10} \, U^3 \, \exp\left(-\frac{z}{z_e}\right), \tag{12}$$

where U is wind speed and z_e is the characteristic depth scale of 0.7 to 1.5 m. The exponential depth dependence has also been observed by others.[29] The distribution of wind speed over the ocean varies with location,[30,31] with annual average values that are generally between 4 and 13 m s^{-1}.[30,31] Near-surface void fraction for mean winds would range between 3×10^{-8} and 10^{-6} in this model. The probability of low winds at any location can be approximated by a Weibull distribution with parameters taken from the maps of Monahan.[30] As an example, we consider a system designed to have sufficient SNR when $F_v > 10^{-8}$. This system would have sufficient SNR 99.6% of the time in the windiest regions, but only 60% of the time in the calmest regions. The region of operation needs to be considered in system design.

One difference between the laboratory experiment and a field system is that the latter must work through the sea surface. One consequence of this is that a fraction of the incident light will be blocked by whitecaps and foam, especially at high wind speeds. The fraction of the surface covered by whitecaps and foam can be estimated from the wind speed as $3.84 \times 10^{-6} \, U^{3.41}$.[32] Less than 10% of the incident light will be blocked by whitecaps and foam unless the wind speed is >20 m s^{-1}; winds this high are not common,[30] so this is not a serious limitation.

Another consequence of the surface is that waves can introduce fluctuations in the signal.[33] These could be important when there is a surface wave whose wavelength, λ, is equal to the ratio of the aircraft speed across the waves to the acoustic frequency of interest, or

$$\lambda = \frac{v \, \cos(\theta)}{f}, \tag{13}$$

where v is the aircraft speed and θ is the angle between the aircraft direction and the direction of propagation of wave. At the low end of the audio range (20 Hz), the important wavelength will be between 2.5 and 5 m for $\theta = 0$ and typical aircraft speeds between 50 and 100 m s^{-1}. At higher frequencies or greater angles between the aircraft and wave directions, the important surface wavelength becomes smaller. When this wavelength becomes smaller than the size of the laser illumination on the surface, the effects will be reduced by averaging over multiple surface waves.

The detection of blue whales (*Balaenoptera musculus*) in the Southern Ocean provides an example of system performance in the open ocean. These whales produce sound in a frequency band of 25 to 29 Hz with source strength of 189 ± 3 dB re 1 μPa at 1 m with an empirically determined propagation loss of $17.8 \log(r)$, where r is the range in meters.[34] Similar source strengths have been measured for these animals at other locations.[35–37] Assuming that this signal

will be detectable if the modulation depth is above the standard deviation of receiver noise, we can calculate the required SNR as a function of range. From Eq. (10), we have the requirement for this example that SNR > 34 dB $+ 17.8 \log(r)$.

To obtain an idea of the feasibility of such a measurement, we calculated the SNR to be expected from an airborne lidar using parameters that are readily achievable (Table 1). Assuming that this lidar is limited by shot noise in the photocurrent, it will have an SNR of 110 dB. Thus, detection of blue whales should be possible at any depth where they are likely to be found[38] and out to horizontal ranges over 18 km. This is in sharp contrast to other aerial remote sensing techniques that require whales to be very close to the surface.[39] Background noise levels at these frequencies are generally determined by shipping noise.[40–42] Recent measurements that include high shipping noise are 85 dB (Ref. 42) and 91 dB (Ref. 41) for a 4 Hz bandwidth. Shipping noise has increased, and the upper limit of older measurements is below 70 dB.[40] All of these background levels are well below the 113 dB signal level at the 18 km range.

For an aircraft speed of 60 m s^{-1}, waves on the surface, foam patches, or spatial structures in the bubble distribution with wavelengths of 2 to 2.5 m will be detected as acoustic signatures in the 25 to 29 Hz band. These effects can be mitigated by using a wide lidar beam. While the fluctuations of the irradiance in the water can be very large,[33] the total lidar backscatter will be much smaller since fluctuations from features smaller than the beam will be spatially averaged.[43,44] A complete design analysis is beyond the scope of this paper, but we should note that measurement depth would be a consideration for this and other low-frequency applications. Wave-induced fluctuations decrease with measurement depth,[44] and both wave-induced fluctuations and bubble void fraction increase with wind speed. This suggests that the optimum measurement depth would increase with increasing wind speed.

Another example of interest is the detection of the acoustic pinger (e.g., Teledyne Benthos ELP-362D) from the flight data recorder on an aircraft that is lost over the ocean. The pinger transmits a series of 9 ms long pulses of sound at a frequency of 37.5 kHz with source strength of 160.5 dB re 1 μPa at 1 m. At this frequency, the absorption is ~5 dB per km, which must be added to the geometric propagation loss. This would take a much larger lidar system, perhaps similar to that in Table 1, and a larger void fraction. The requirement for larger void fraction means that the system would need to scan the ocean surface for the large returns associated with bubble plumes. When it found one, it would need to track that position on the surface as long as possible to capture the ping. That time could be as long as a second. The result, assuming a plume with a void fraction of 10^{-4}, is an SNR of 154 dB and detection to a range of 4 km. Background noise level at this frequency is generally determined by wind speed through breaking waves and bubbles. Typical recent values in a 100 Hz bandwidth are 53 dB[45] to 63 dB[42] for sea state six (wind 11 to 14 m s^{-1}), well below the pinger signal level of 140.5 dB at 4 km.

Table 1 Lidar parameters used for signal-to-noise ratio calculations.

Parameter	Whale	Pinger
Wavelength	532 nm	532 nm
Pulse energy	1 mJ	100 mJ
Pulse repetition rate	100 Hz	100 kHz
Flight altitude	100 m	100 m
Bubble void fraction	10^{-7}	10^{-4}
Receiver telescope diameter	20 cm	50 cm
Receiver transmission	0.1	0.1
Detector quantum efficiency	0.1	0.1
Receiver noise bandwidth	4 Hz	100 Hz

Aliasing of spatial variability at this frequency can also be neglected, since the spatial wavelength would be ~2 mm.

While it would seem that scanning the lidar to increase the swath width would improve pinger detection probability and aid in localizing the source, this is probably not useful. As a practical matter, the lidar zenith angle is limited to ~45 deg before surface reflection losses become large. This implies a swath width of about twice the altitude, or 200 m in our example. Depending on pinger depth, the region of detectable signal on the surface may be several kilometers across. The horizontal detection range, the sum of the detectable signal radius and swath radius, is almost completely determined by the signal radius in this case. Note also that localizing the source to within a few kilometers is adequate for this application. A surface vessel can quickly locate and recover the flight recorder within this small area.

6 Conclusions

The main conclusion is that underwater sound can be detected from above the surface by lidar when bubbles are present. Theoretical estimates of the resulting modulation depth were confirmed by laboratory experiment with a controlled acoustic source at two different bubble void fractions. Scaling these results to a field system with typical parameters suggests that blue whale calls should be detectable at horizontal ranges of up to 18 km in the Southern Ocean. A much larger system could be added to the aircraft that searches the ocean surface for debris after a plane crash that would simultaneously listen for the pinger on the flight data recorder.

Acknowledgments

References

1. A. L. Fabrikant, "Modulated opto-acoustical sounding of the upper ocean," *Int. J. Remote Sens.* **18**(11), 2277–2287 (1997).
2. A. D. Matthews and L. L. Arrieta, "Acoustic optic hybrid (AOH) sensor," *J. Acoust. Soc. Am.* **108**(3), 1089–1093 (2000).
3. L. Antonelli and F. Blackmon, "Experimental demonstration of remote, passive acousto-optic sensing," *J. Acoust. Soc. Am.* **116**(6), 3393–3403 (2004).
4. L. Antonelli and F. Blackmon, "Experimental investigation of optical, remote, aerial sonar," in *OCEANS '02 MTS/IEEE*, Vol. 4, pp. 1949–1955 (2002).
5. I. B. Esipov and Y. S. Pashin, "Acoustooptic interaction on a statistically rough surface," *Soviet Phys. Acoust.* **36**(3), 240–244 (1990).
6. J. H. Churnside et al., "Effects of underwater sound and surface ripples on scattered laser light," *Acoust. Phys.* **54**(2), 204–209 (2008).
7. M. V. Trevorrow, "Measurements of near-surface bubble plumes in the open ocean with implications for high-frequency sonar performance," *J. Acoust. Soc. Am.* **114**(5), 2672–2684 (2003).
8. S. A. Thorpe, "On the clouds of bubbles formed by breaking wind-waves in deep water, and their role in air: sea gas transfer," *Philos. Trans. R. Soc. A* **304**(1483), 155–210 (1982).
9. M. Minnaert, XVI, "On musical air-bubbles and the sounds of running water," *Philos. Mag. Ser. 7* **16**(104), 235–248 (1933).
10. J. H. Churnside, "Lidar signature from bubbles in the sea," *Opt. Express* **18**(8), 8294–8299 (2010).
11. M. V. Trevorrow, B. Vasiliev, and S. Vagle, "Directionality and maneuvering effects on a surface ship underwater acoustic signature," *J. Acoust. Soc. Am.* **124**(2), 767–778 (2008).
12. J. K. Allen et al., "Radiated noise from commercial ships in the Gulf of Maine: implications for whale/vessel collisions," *J. Acoust. Soc. Am.* **132**(3), EL229–EL235 (2012).
13. J. A. Puleo, R. V. Johnson, and T. N. Kooney, "Laboratory air bubble generation of various size distributions," *Rev. Sci. Instrum.* **75**(11), 4558–4563 (2004).

14. E. D. Brown et al., "Remote sensing of capelin and other biological features in the North Pacific using lidar and video technology," *ICES J. Mar. Sci.* **59**(5), 1120–1130 (2002).
15. P. Carrera et al., "Comparison of airborne lidar with echosounders: a case study in the coastal Atlantic waters of southern Europe," *ICES J. Mar. Sci.* **63**(9), 1736–1750 (2006).
16. J. H. Churnside and P. L. Donaghay, "Thin scattering layers observed by airborne lidar," *ICES J. Mar. Sci.* **66**(4), 778–789 (2009).
17. J. H. Churnside et al., "Airborne lidar detection and characterization of internal waves in a shallow fjord," *J. Appl. Remote Sens.* **6**(1), 063611 (2012).
18. L. S. Dolin, I. S. Dolina, and V. A. Savel'ev, "A lidar method for determining internal wave characteristics," *Izv. Atmos. Ocean. Phys.* **48**(4), 444–453 (2012).
19. J. H. Churnside and L. A. Ostrovsky, "Lidar observation of a strongly nonlinear internal wave train in the Gulf of Alaska," *Int. J. Remote Sens.* **26**(1), 167–177 (2005).
20. J. H. Lee et al., "Oceanographic lidar profiles compared with estimates from in situ optical measurements," *Appl. Opt.* **52**(4), 786–794 (2013).
21. J. H. Churnside, "Polarization effects on oceanographic lidar," *Opt. Express* **16**(2), 1196–1207 (2008).
22. E. J. Terrill, W. K. Melville, and D. Stramski, "Bubble entrainment by breaking waves and their influence on optical scattering in the upper ocean," *J. Geophys. Res. Oceans* **106**(C8), 16815–16823 (2001).
23. G. B. Deane and M. D. Stokes, "Scale dependence of bubble creation mechanisms in breaking waves," *Nature* **418**(6900), 839–844 (2002).
24. E. Lamarre and W. K. Melville, "Void-fraction measurements and sound-speed fields in bubble plumes generated by breaking waves," *J. Acoust. Soc. Am.* **95**(3), 1317–1328 (1994).
25. S. Thorpe et al., "Bubble clouds and Langmuir circulation: observations and models," *J. Phys. Oceanogr.* **33**(9), 2013–2031 (2003).
26. S. Vagle, J. Gemmrich, and H. Czerski, "Reduced upper ocean turbulence and changes to bubble size distributions during large downward heat flux events," *J. Geophys. Res. Oceans* **117**(C7), C00H16 (2012).
27. J. Gemmrich, "Bubble-induced turbulence suppression in Langmuir circulation," *Geophys. Res. Lett.* **39**(10), L10604 (2012).
28. G. B. Crawford and D. M. Farmer, "On the spatial distribution of ocean bubbles," *J. Geophys. Res. Oceans* **92**(C8), 8231–8243 (1987).
29. M. J. Buckingham, "Sound speed and void fraction profiles in the sea surface bubble layer," *Appl. Acoust.* **51**(3), 225–250 (1997).
30. A. H. Monahan, "The probability distribution of sea surface wind speeds. Part I: theory and seawinds observations," *J. Clim.* **19**(4), 497–520 (2006).
31. S. B. Capps and C. S. Zender, "Observed and CAM3 GCM sea surface wind speed distributions: characterization, comparison, and bias reduction," *J. Clim.* **21**(24), 6569–6585 (2008).
32. E. C. Monahan and I. Muircheartaigh, "Optimal power-law description of oceanic whitecap coverage dependence on wind speed," *J. Phys. Oceanogr.* **10**(12), 2094–2099 (1980).
33. T. Dickey et al., "Introduction to special section on recent advances in the study of optical variability in the near-surface and upper ocean," *J. Geophys. Res. Oceans* **117**(C7), C00H20 (2012).
34. A. Širović, J. A. Hildebrand, and S. M. Wiggins, "Blue and fin whale call source levels and propagation range in the Southern Ocean," *J. Acoust. Soc. Am.* **122**(2), 1208–1215 (2007).
35. M. A. McDonald et al., "The acoustic calls of blue whales off California with gender data," *J. Acoust. Soc. Am.* **109**(4), 1728–1735 (2001).
36. A. M. Thode, G. L. D'Spain, and W. A. Kuperman, "Matched-field processing, geoacoustic inversion, and source signature recovery of blue whale vocalizations," *J. Acoust. Soc. Am.* **107**(3), 1286–1300 (2000).
37. W. C. Cummings and P. O. Thompson, "Underwater sounds from the blue whale, Balaenoptera musculus," *J. Acoust. Soc. Am.* **50**(4B), 1193–1198 (1971).
38. D. A. Croll et al., "The diving behavior of blue and fin whales: is dive duration shorter than expected based on oxygen stores?," *Comp. Biochem. Physiol. A Mol. Integr. Physiol.* **129**(4), 797–809 (2001).

39. J. Churnside, L. Ostrovsky, and T. Veenstra, "Thermal footprints of whales," *Oceanography* **22**(1), 206–209 (2009).
40. G. M. Wenz, "Acoustic ambient noise in the ocean: spectra and sources," *J. Acoust. Soc. Am.* **34**(12), 1936–1956 (1962).
41. M. A. McDonald, J. A. Hildebrand, and S. M. Wiggins, "Increases in deep ocean ambient noise in the Northeast Pacific west of San Nicolas Island, California," *J. Acoust. Soc. Am.* **120**(2), 711–718 (2006).
42. P. H. Dahl et al., "Underwater ambient noise," *Acoust. Today* **3**(1), 23–33 (2007).
43. J. H. Churnside, V. V. Tatarskii, and J. J. Wilson, "Oceanographic lidar attenuation coefficients and signal fluctuations measured from a ship in the Southern California Bight," *Appl. Opt.* **37**(15), 3105–3112 (1998).
44. J. H. Churnside and J. J. Wilson, "Power spectrum and fractal dimension of laser backscattering from the ocean," *J. Opt. Soc. Am. A* **23**(11), 2829–2833 (2006).
45. A. R. Childers, T. E. Whitledge, and D. A. Stockwell, "Seasonal and interannual variability in the distribution of nutrients and chlorophyll a across the Gulf of Alaska shelf: 1998–2000," *Deep Sea Res. Part 2 Top. Stud. Oceanogr.* **52**(1–2), 193–216 (2005).

James H. Churnside received his PhD from the Oregon Graduate Center in 1978, after which he joined the technical staff of The Aerospace Corporation. In 1985, he joined the NOAA Environmental Technology Laboratory, now the Earth System Research Laboratory, where he is currently developing airborne instrumentation for marine ecosystem studies. He has published 96 articles in refereed journals and holds four patents. He is a fellow of OSA and SPIE.

Konstantin Naugolnykh is a senior scientist at the National Oceanic and Atmospheric Administration, Earth System Research Laboratory and Zel Technologies, LLC. He received his PhD in physics at the N. N. Andreev Acoustics Institute of the USSR Academy of Sciences in 1959. In 1963, he worked in the Physics Department at Brown University on parametric radiation studies. He is a member of the Russian Acoustical Society and a Fellow of the Acoustical Society of America.

Richard D. Marchbanks is a senior associate scientist at the Cooperative Institute for Research in Environmental Sciences (CIRES) at the University of Colorado. His primary expertise is lidar and optical systems for remote sensing. Research includes development and application of ultraviolet differential absorption lidar (DIAL) systems, infrared wind lidar systems and ocean probing lidar systems. Richard earned his MS in Electro-Optical Engineering from the University of New Mexico in 1995.